Molecular Vision 2020; 26:705-717 <http://www.molvis.org/molvis/v26/705>
Received 7 July 2020 | Accepted 8 October 2020 | Published 10 October 2020

© 2020 Molecular Vision

An optimized protocol for retina single-cell RNA sequencing

Benjamin R. Fadl,[1] Seth A. Brodie,[2] Michael Malasky,[2] Joseph F. Boland,[2] Michael C. Kelly,[3] Matthew W. Kelley,[4] Erich Boger,[5] Robert Fariss,[6] Anand Swaroop,[1] Laura Campello[1]

[1]Neurobiology, Neurodegeneration & Repair Laboratory, National Eye Institute, National Institutes of Health, Bethesda, MD; [2]Division of Cancer Epidemiology and Genetics, National Cancer Institute, National Institutes of Health & NCI-Frederick, Leidos Biomedical Research Inc., Frederick, MD; [3]Single Cell Analysis Facility, Cancer Research Technology Program, Frederick National Laboratory, Bethesda, MD; [4]Laboratory of Cochlear Development, National Institute on Deafness and Other Communication Disorders, National Institutes of Health, Bethesda, MD; [5]Genomics and Computational Biology Core, National Institute on Deafness and Other Communication Disorders, National Institutes of Health, Bethesda, MD; [6]Biological Imaging Core, National Eye Institute, National Institutes of Health, Bethesda, MD

Purpose: Single-cell RNA sequencing (scRNA-seq) is a powerful technique used to explore gene expression at the single cell level. However, appropriate preparation of samples is essential to obtain the most information out of this transformative technology. Generating high-quality single-cell suspensions from the retina is critical to preserve the native expression profile that will ensure meaningful transcriptome data analysis.
Methods: We modified the conditions for rapid and optimal dissociation of retina sample preparation. We also included additional filtering steps in data analysis for retinal scRNA-seq.
Results: We report a gentle method for dissociation of the mouse retina that minimizes cell death and preserves cell morphology. This protocol also results in detection of higher transcriptional complexity. In addition, the modified computational pipeline leads to better-quality single-cell RNA-sequencing data in retina samples. We also demonstrate the advantages and limitations of using fresh versus frozen retinas to prepare cell or nuclei suspensions for scRNA-seq.
Conclusions: We provide a simple yet robust and reproducible protocol for retinal scRNA-seq analysis, especially for comparative studies.

The development of RNA sequencing (RNA-seq) technology has allowed researchers to examine complex biologic processes by mapping and quantifying transcripts under different conditions, such as physiologic or disease states [1-3]. However, bulk RNA-seq measures the average expression of genes per tissue or cell culture, generally masking the cell-to-cell variability and making it particularly difficult to analyze minor cell subpopulations. Single-cell RNA sequencing (scRNA-seq) has emerged as a revolutionary tool to overcome this problem by providing unprecedented opportunities for exploring gene expression profiles at the single-cell level [4,5].

Recent scRNA-seq studies have provided a comprehensive transcriptome atlas of the human fetal and adult retina [6,7], including comparative analyses of gene expression of central (fovea and macula) and peripheral specific cell types in the primate and human retina [8,9]. Transcriptome analyses have also dissected the complexity of human retinal organoids at different developmental stages [7,10-12]. Similarly, scRNA-seq investigations have revealed the diversity in the fetal and adult mouse retina, as well as retinal organoids from mouse pluripotent stem cells [13]. scRNA-seq has also been used to characterize and classify cell types of the retina, allowing us to expand previous knowledge and identify undescribed cell types [14-16]. Analyses of retina transcriptomes at single-cell resolution have uncovered cell-type gene expression signatures in response to hypoxia and inflammatory conditions [17,18]. However, despite considerable progress, significant challenges remain in the dissociation and analysis of scRNA-seq data of retina samples, especially for comparative studies.

Isolation of single cells is a critical step in any single-cell transcriptome investigation. Preparing cell suspensions is relatively straightforward for cell lines or blood samples; however, it can be a major hurdle for tissue samples. Thus, to provide retinal cell suspensions that preserve the native expression profile, the selection of an optimal protocol for tissue dissociation should be addressed carefully. Optimal dissociation needs to achieve a balance between isolating cell types that are difficult to dissociate while avoiding damage to those that are fragile. Papain-based enzymatic protocols have been shown to successfully dissociate retinal tissue and have been applied in numerous scRNA-seq studies of retina tissue and organoids [5,6,8-11,13,14,17,19,20]. Nonetheless, special

Correspondence to: Laura Campello, Neurobiology, Neurodegeneration & Repair Laboratory, National Eye Institute, National Institutes of Health, Building 6, Room 308, 6 Center Drive, Bethesda, MD, 20892; Phone: (301) 827-6093; FAX: (301) 480-9917; email: laura.campello@nih.gov

attention should be paid to several parameters in the dissociation protocol that compromise the viability of the cells and potentially impact the quality of the scRNA-seq data.

The mammalian retina is a complex tissue formed by multiple types of interconnected neurons and glial cells, with photoreceptors the most abundant cell type [21,22]. In the mouse retina, rod photoreceptors account for more than 70% of all retinal cells. Photoreceptor cells contain a highly specialized outer segment where phototransduction takes place, which is joined to the cell body by a very fragile connecting cilium [23]. The structural fragility of photoreceptors makes them sensitive to enzymatic and mechanical dissociation protocols causing RNA leakage from damaged cells. This ambient RNA present in cell suspensions can be incorporated into scRNA-seq microfluidic droplets and contaminate other cell types, making it difficult to identify cell types confidently. This contamination can largely influence scRNA-seq results, especially in rod-dominant retina samples. In addition, this problem should be minimized in cases of highly expressed genes, as is the case of rhodopsin in rod cells, to avoid confounding cell clustering.

In this study, we demonstrate the efficacy of an optimized gentle protocol for retina dissociation that decreases cell death and preserves cell morphology, resulting in a higher number of genes detected per cell. We also created an optimized scRNA-seq bioinformatic analysis pipeline that removes low-quality cells and reduces technical noise from ambient RNA contamination. Finally, we provide a comparative analysis of different methodologies for single cell or single nucleus profiling in retina samples.

METHODS

Mouse lines and animal husbandry: C57BL/6J and the transgenic *Nrl-L-EGFP/Grm6-tdTomato* mouse strains were used in this study. The transgenic *Nrl-L-EGFP/Grm6-tdTomato* strain was generated by crossing the in-house *Nrl-L-EGFP* mouse [24] with the *mGluR6-tdTomato* mouse (also known as *Grm6-tdTomato*) [25], kindly provided by Dr. Rachel O. Wong (University of Washington, Seattle). Mice, both male and female, were maintained in National Institutes of Health (NIH) animal care facilities in controlled ambient illumination on a 12 h:12 h light-dark cycle. The studies conformed to the ARVO statement for the Use of Animals in Ophthalmic and Vision Research. Animal protocols were approved by the National Eye Institute (NEI) Animal Care and Use Committee (NEI-ASP#650).

Vibratome sectioning and fluorescence imaging of the retina: Animals were euthanized via CO_2 inhalation in accordance with NIH ARAC "Guidelines for the Euthanasia of rodents Feti and Neonates". Euthanasia was confirmed by cervical dislocation. Eyes of 3-month-old *Nrl-L-EGFP/Grm6-tdTomato* transgenic mice were enucleated, and the whole eyes were fixed in 4% (w/v) paraformaldehyde in PBS (1X; 137 mM NaCl, 2.7 mM KCl, 8 mM Na_2HPO_4, and 2 mM KH_2PO_4, pH 7.4) for 2 h at room temperature. After washing in PBS, the cornea, lens, and vitreous body were removed, and then the eyecups were embedded in agar, cut at 100 µm on a Leica VT1000S vibratome (Wetzlar, Germany), and collected in PBS. The retina sections were mounted on slides, and images of the endogenous fluorescence were taken using a Zeiss LSM 880 confocal microscope (Jena, Germany).

Solutions for retina dissociation:

Digestion solution—Hank's Buffered Salt Solution (HBSS; H8264–1L, Sigma-Aldrich, St. Louis, MO) supplemented with 5.5 mM glucose (G7021–100G, Sigma-Aldrich), 5.7 mM cysteine (C562–25, Fisher Scientific, Hampton, NH), and 40 U/ml papain (LS003119, Worthington Biochemical, Lakewood, NJ) was titrated to pH 6.5 using potassium hydroxide (KOH) and then incubated for 30 min at 37 °C. After incubation, 10 mM HEPES buffer (SKU# 15,630-106, Invitrogen, Carlsbad, CA) was added to the solution, and it was titrated to pH 7.4 using KOH. About 120 U/ml DNase I (LS006333, Worthington Biochemical), 10 U/ml superoxide dismutase (LS003540, Worthington Biochemical), 10–25 U/ml catalase (C1345–1G, Sigma-Aldrich), and 0.02 mM D-alpha-tocopherol acetate (T1157–1G, Sigma-Aldrich) were added before the solution was filtered using a 0.22 µm pored sterile filter.

Inactivation solution—HBSS supplemented with 11 mM glucose and 10 mM HEPES buffer was titrated to pH 7.4 with KOH. Subsequently, 120 U/ml DNase I, 0.07 mM antipain (A6191–25MG, Sigma-Aldrich), 10 U/ml superoxide dismutase, 10–25 U/ml catalase, and 0.02 mM D-alpha-tocopherol acetate were added, and the solution was sieved using a 0.22 µm pored sterile filter.

Washing solution—HBSS supplemented with 11 mM glucose, 0.04% bovine serum albumin (BSA; A8806–5G, Sigma-Aldrich) and 10 mM HEPES buffer was titrated to pH 7.4 before the solution was sieved using a 0.22 µm pored sterile filter.

Protocols for retina dissociation:

Frequently used protocol—Retinas were dissected in fresh cold (4 °C) 1X Dulbecco's PBS (DPBS; D8537–500ML, Sigma-Aldrich), transferred to a 5 ml polypropylene round-bottom tube, and promptly dissociated with a commonly

used papain dissociation protocol (Worthington Biochemicals) with minor modifications. Briefly, single retinas were incubated in 1 ml of digestion solution at 37 °C for 10 min. Mechanical trituration was performed by pipetting 30 times with a P1000 pipette. Cells were centrifuged, using a swing-bucket rotor, at 300 ×*g* for 5 min at 4 °C, and the digestion solution was removed. The dissociated cells were gently resuspended in 700 µl of inactivation solution prewarmed for 10 min at 28 °C. Then, 700 µl of chilled washing solution was layered under the cell suspension, and the cells were centrifuged at 300 ×*g* for 5 min at 4 °C. After the washing solution was removed, cells were resuspended in 500 µl of DPBS containing 0.04% BSA and passed through a 40 µm cell strainer (pluriSelect, Leipzig, Germany).

The optimized protocol—The retinas were dissected in fresh and cold 1X HBSS and individually transferred to a 5 ml polypropylene round-bottom tube containing 1 ml of digestion solution. The samples were then incubated at 8 °C for 40 min followed by a second incubation at 28 °C for 10 min. The tube was inverted gently every 10 min during the long incubation and after 5 min during the short incubation. After the incubation steps, the retina, which remained morphologically intact, sank to the bottom of the tube. The digestion solution was discarded by pipetting without disturbing the retina. Mechanical trituration of the retina was performed in 700 µl of prewarmed (10 min at 28 °C) inactivation solution by pipetting slowly 10 to 15 times with a flame polished glass Pasteur pipette mounted on a P1000 pipette tip. The solution was aspirated and slowly released along the tube wall. Trituration was stopped when the retina was visibly dissociated, and 700 µl of ice-cold washing solution was layered under the cell suspension. Cell suspensions were centrifuged using a swing-bucket rotor at 200 ×*g* for 5 min at 4 °C. After the supernatant was removed, the cells were resuspended in 500 µl of DPBS containing 0.04% BSA and passed through a 40 µm cell strainer (pluriSelect).

Flow cytometry analysis of dissociated retinas: Adult retinas from transgenic *Nrl-L-EGFP/Grm6-tdTomato* mice were dissociated following the frequently used protocol or the optimized protocol (four or five biologic replicates were analyzed for each protocol). Cell suspensions were filtered through a 45-µm strainer (BD Biosciences, San Diego, CA) to prevent clumps. Cellular viability was determined by measuring the capacity of the cells to exclude the vital dye 4′,6-diamidino-2-phenylindole (DAPI). Each retina was examined separately in a BD FACSAria™ Fusion flow cytometer (BD Biosciences), and a total of 200,000 cells were acquired per retina. Data were analyzed with FACSDiva software (BD Biosciences). A two-way analysis of variance (ANOVA) multiple comparisons test was performed to examine differences in cell viability and the number of EGFP versus tdTomato living cells between the two protocols used for tissue dissociation. A p value of less than 0.05 was considered statistically significant.

Morphological characterization of cell suspensions: To determine the efficiency of the optimized protocol for retina dissociation, we performed morphological assessment of retinal cell suspensions from adult *Nrl-L-EGFP/Grm6-tdTomato* transgenic mice and compared them to the frequently used protocol described previously. Dissociated live cell suspensions from both protocols were deposited on µ-Slide 8-well coverslip-like bottom chambers (Ibidi, Martinsried, Planegg, Germany) and imaged with a Zeiss LSM 880 confocal microscope. Efficiency was evaluated with quantification and statistical comparison of preservation of retinal cell morphologies. The percentage of cells exhibiting neuronal morphology traits versus rounded-shaped in suspensions was determined for rods (EGFP-positive cells) and ON bipolar cells (tdTomato-positive cells) after evaluation of a minimum of 200 cells per protocol and cell type (two or three biologic replicates per protocol). Cells were assigned to one of three distinct categories according to the degree of general morphological preservation. The rod categories were preserved inner or outer segments, axons, or round shape. The ON bipolar cell categories were preserved axon and dendrites, only axon or round shape. A two-way ANOVA multiple comparisons test was performed to examine differences in morphology among living cells obtained from the two protocols for tissue dissociation. A p value of less than 0.05 was considered statistically significant.

Methanol fixation of cells: We applied the updated Methanol Fixation of Cells for Single Cell RNA Sequencing protocol (Rev D) from 10x Genomics (Pleasanton, CA) [26] to the retinal cells obtained after we followed the optimized protocol for dissociation. Briefly, using a wide-bore pipette tip, 2 ml chilled 1X DPBS were added to the cell pellet. Cells were resuspended with a gentle pipette mix ten times or until the cells were resuspended. The cell suspension was equally divided in two 5 ml polypropylene round-bottom tubes, approximately 1–2 × 10^6 cells per tube. The cells were centrifuged, using a swing-bucket rotor, at 300 ×*g* for 5 min at 4 °C. The supernatant was removed without disrupting the pellet, and the cells were resuspended in 1 ml chilled 1X DPBS. After centrifuging at 300 ×*g* for 5 min at 4 °C, the supernatant was removed, and the cells were resuspended in 400 µl of chilled 1X DPBS (200 µl 1X DPBS/1 × 10^6 cells) using a wide-bore pipette tip. About 1.6 ml of chilled 100% methanol (800 µl methanol/1 × 10^6 cells) was added drop

by drop while the cell suspension was gently stirred. The samples were stored at −20 °C for 5 days. Fixed cells were centrifuged at 1,000 ×*g* for 5 min at 4 °C, and the cells were rehydrated in 500 µl rehydration buffer (3X saline sodium citrate (SSC) buffer supplemented with 0.04% BSA, 1 mM DTT, and 0.2 U/µl RNase inhibitor) with a gentle pipette mix using a regular-bore tip.

Single nuclei isolation: Single nuclei suspensions were generated following a detergent-based lysis protocol [27] with minor modifications. Briefly, two retinas were dissected in fresh and cold 1X HBSS and flash frozen on dry ice. Retinas were lysed in 500 µl of detergent lysis buffer (0.32 M sucrose, 10 mM HEPES (pH = 8.0), 5 mM calcium chloride, 3 mM magnesium chloride, 0.1 mM EDTA, 1 mM DTT, and 0.1% Triton-X) using a Dounce homogenizer. After 1 ml of low sucrose buffer (0.32 M sucrose, 10 mM HEPES (pH = 8.0), 5 mM calcium chloride, 3 mM magnesium chloride, 0.1 mM EDTA, and 1 mM DTT) was added and pipette mixed, the whole lysate was passed through a 40 µm cell strainer (pluriSelect). Two milliliters of low sucrose buffer were used to wash the mesh of the cell strainer. The sample, containing a total of 3.5 ml of solution, was centrifuged at 3,200 ×*g* for 10 min at 4 °C, and the supernatant was decanted. The pellet containing the nuclei was resuspended in 500 µl of low sucrose buffer and homogenized using an electric homogenizer for 20 s. Two milliliters of sucrose density buffer (1 M sucrose, 10 mM HEPES (pH = 8), 3 mM magnesium chloride, and 1 mM DTT) were deposited at the bottom of the tube, and the samples were centrifuged at 3,200 ×*g* for 20 min at 4 °C. The supernatant was decanted, and the pellet, containing the nuclei, was suspended in 200 µl of resuspension solution (DPBS supplemented with 4% BSA and 0.2 U/µl RNase Inhibitor) and passed through a 20 µm strainer (pluriSelect).

Single-cell transcriptomic platform (10x Genomics Chromium system): For each retina sample, 2-month-old C57BL/6J mice, scRNA-seq or snRNA-seq data were generated using the 10x Genomics Chromium platform. Single cell or nuclei suspensions were loaded onto the Chromium Single Cell system using the v2 (Chromium Single Cell 3′ Library and Gel Bead Kit v2) or v3.1 (Chromium Next GEM Single Cell 3′ GEM, Library and Gel Bead Kit v3.1) chemistry. The manufacturer's instructions were followed with minor modifications. Cell concentration and viability counts were estimated using the Cellometer Auto 2000 Cell Viability Counter (Nexcelom Bioscience, Lawrence, MA). Cells were diluted to achieve 900–1,400 cells/µl. Based on previous analysis, we subtracted 200–300 cells/µl from the calculated cell concentration to account for debris falsely counted as cells. Approximately 17,000 live cells per sample were loaded into the Chromium chip following the Cell Suspension Volume Calculator Table to capture transcripts from approximately 10,000 cells. For every elution step in the cDNA amplification and library construction protocols, the elution volume was increased by 3 µl (Elution solution I or elution buffer [EB; 19086, Qiagen, Germantown, MD]) to obtain a supernatant that was devoid of contaminating SPRI magnetic beads. We used 12 cycles for the cDNA amplification reaction in v2 and v3.1 chemistry. Libraries were quantified using the Kapa library quantification kit from Roche (Basel, Switzerland) and sequenced on a NovaSeq 6000 (Illumina, San Diego, CA).

Bioinformatics pipeline: Primary analysis of the raw sequencing data was processed through the Cell Ranger pipeline (v3.1.0, 10x Genomics) using cellranger mkfastq and cellranger count with default settings and the provided mouse reference (refdata-cellranger-mm10–3.0.0). Secondary analysis consisting of normalization, scaling, dimension reduction, and clustering was performed using the R-package Seurat (v3.1) [28,29] following the publisher's vignette using sctransform (compiled April 17, 2020) [30]. Imported data were subsequently processed using default settings for principal component analysis (PCA) dimensionality reduction, graph-based clustering, and uniform manifold approximation and projection (UMAP) embedding through the following functions: SCTransfrom() > RunPCA() > RunUMAP() > FindNeighbors() > FindClusters(). The selection of which principal components was estimated using EllbowPlot() for each sample individually. Cell type identity was determined for each resulting cluster by generating Violin plots for known cell markers [8]. Independently, a second round of cell type identification was performed by using the function AddModuleScore() using the same cell marker list. Cell types were assigned based on the highest score for each cell individually. Cell filtering was performed with two criteria: (a) Cells with a less than threefold change between the highest and second highest score, and (b) rods in non-rod cluster were excluded. The remaining cells were then reprocessed as previously described. A final filter for remaining ambiguous cells between the cluster-wide and score-based cell type identification was applied.

The snRNA-seq data were processed similarly to the scRNA-seq data with the following differences. We generated a custom reference for pre-mRNA that allows reads mapped to introns to be counted, following the 10x Genomics instructions Generating a Cell Ranger Compatible pre-mRNA Reference Package. We did not apply score-based cell type assignment and fold-change filtering, because of high expression of a few rod genes.

RESULTS

Dissociation of the retina for scRNA-seq studies: Frequently used protocols for mouse retina dissociation digest the tissue by incubation with activated papain at 37 °C for 10–15 min, followed by trituration [13,17,18]. Our initial scRNA-seq analyses of retinal samples dissociated by following this protocol led to high contamination of rhodopsin in several cell clusters, suggesting cytoplasmic mRNA leakage through broken cell membranes. Therefore, we modified the protocol for retina dissociation as follows: (1) reducing papain enzymatic activity (using low temperature during the digestion step), (2) decreasing mechanical cell damage (using a flame polished end glass Pasteur pipette during the trituration step), and (3) alleviating oxidative stress (by adding superoxide dismutase, catalase, and D-alpha-tocopheryl acetate to the digestion and inactivation solutions). The flowchart in Figure 1A shows the steps used for the frequently used and optimized protocols. The transgenic *Nrl-L-EGFP/Grm6-tdTomato* mouse, which expresses EGFP in rod photoreceptors and tdTomato (pseudo-colored magenta) in ON bipolar cells (Figure 1B), was used to evaluate the morphology and viability of retinal cell suspensions from both protocols (Figure 1C). Each image in Figure 1C is composed of a bright-field image of all the cells in the cell suspension, rod photoreceptor cells expressing EGFP (shown in green) and ON bipolar cells expressing tdTomato (pseudo-colored in magenta). The optimized protocol better preserved cell morphology compared to the frequently used protocol. We observed the entire cell morphology of bipolar cells, including dendrites, soma, axon and synaptic terminals, and Müller cells, which exhibited their typical morphological features (vertical stalk and small tangential branches and microvilli) [31] (Simple Anatomy of the Retina by Helga Kolb, 2012; Figure 1D). In addition, we could identify rod and cone outer segments though with general shrinkage (Figure 1D). Compared to the optimized protocol, cells produced by following the frequently used protocol exhibited a general round cell shape (Figure 1C). Specifically, we assessed and quantified morphological changes in rods and ON bipolar cells (EGFP- and tdTomato-positive cells, respectively) in suspension. The optimized protocol revealed improved preservation of cellular morphology, most notably in the ON bipolar cells (Figure 2A). Additional flow cytometry analyses showed that the optimized protocol leads to a higher percentage of cellular viability and an increased proportion of rod cells (Figure 2B). Details of sampling size and description of statistical analyses are provided in methods.

Bioinformatic pipeline for scRNA-seq analysis of retina samples: To reduce the noisy signals generated by RNA leakage from damaged cells, especially from rods, in other cell clusters, we extended the sctransform pipeline in the R package Seurat (Vignette from April 17, 2020) by adding a filtering step after clustering (Figure 3A). Briefly, individual cells were scored based on expression of known cell type-specific genes [8]. Cell type was assigned to individual cells (cluster-independent) according to the highest cell type-associated score. To avoid false positives, cells with less than threefold change between the highest and second highest score were not included in further analysis steps. Rod cells assigned to non-rod clusters were also removed. We repeated the secondary analysis with the raw expression values of the remaining cells including cluster and score-based cell type assignment. Cells with ambiguous cell-type assignment were removed from the final result.

We examined the efficiency of the modified bioinformatic protocol for retina scRNA-seq analysis using publicly available mouse retinal data sets [17]. Figure 3B shows a Sankey diagram comparing the assigned cell type labels using cluster- (left) and score-based (right) pipelines. There was a 10% cell type label mismatch between the two cell type assignment methods, mainly attributed to rod cell signal contaminating other cell clusters (Figure 3C, circle). By using the modified protocol, we were able to considerably reduce the contaminating noise. The UMAP plots in Figure 3C show the cell type assignment for the mouse retina sample before and after the additional filtering step in the modified protocol was applied. The cell type assignment obtained using the modified bioinformatic pipeline reflected more accurately the in vivo cellular composition of the retina [32]. Rod cells accounted for approximately 72% of all cells obtained using the modified pipeline, while the commonly used pipeline determined a 61% rate for the rod population (Figure 3C, percentages).

Sample preparation methods for single-cell studies in the retina: Then, we evaluated the recovery yields, measured as the number of genes detected per cell, of different protocols and methodologies used to prepare the samples for the scRNA-seq studies (Figure 4). We first compared the impact of different retina dissociation protocols on the transcriptome profiles of the individual retinal cell types captured (Figure 4A,B). We found the gene number per cell detected to be increased by up to fourfold using the optimized dissociation protocol compared to the frequently used protocol (Figure 4A,B). Then, we compared the list of genes detected in the majority of cells (≥50%) belonging to the same cell type (Figure 4C). We observed that 193 genes were expressed in at least 50% of rod cells isolated from retinal cell suspensions obtained following the optimized dissociation protocol. However, this number decreased to 33 when we followed the

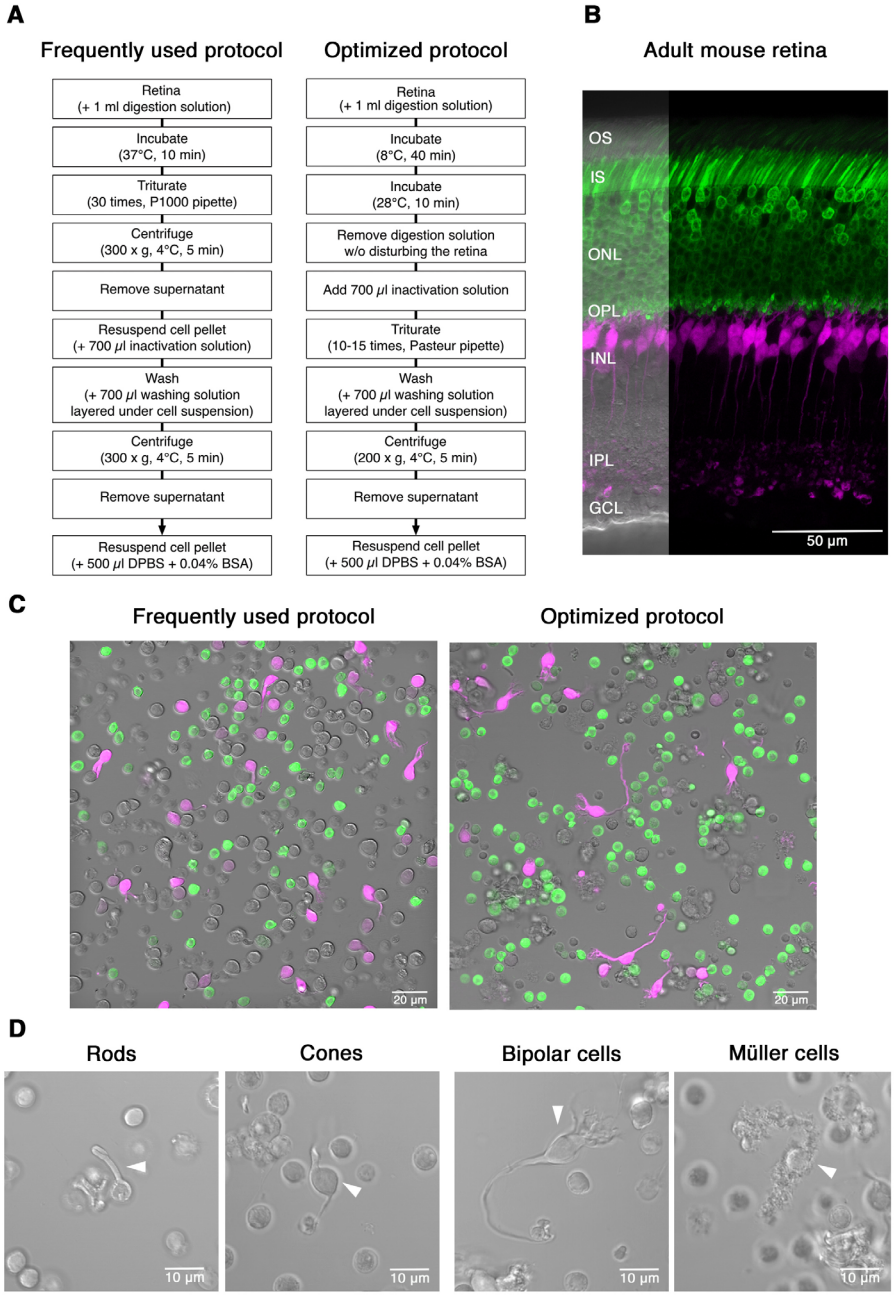

Figure 1. Dissociation of the retina for scRNA-seq. **A**: Flowchart showing different steps of the two protocols for preparing retina cell suspensions. **B**: Vertical section showing EGFP (green) and tdTomato (pseudo-colored in magenta) expression in rods and ON bipolar cells, respectively, in the *Nrl-L-EGFP*/*Grm6-tdTomato* transgenic mouse retina. OS: outer segment; IS: inner segment; ONL: outer nuclear layer; OPL: outer plexiform layer; INL: inner nuclear layer; IPL: inner plexiform layer; GCL: ganglion cell layer. **C**: Representative images of cell suspensions derived from the *Nrl-L-EGFP*/*Grm6-tdTomato* transgenic mouse retina following a frequently used protocol and the optimized protocol for single-cell RNA sequencing (scRNA-seq) sample preparation. **D**: Higher magnification images of rods, cones, and bipolar and Müller cells obtained with the optimized protocol.

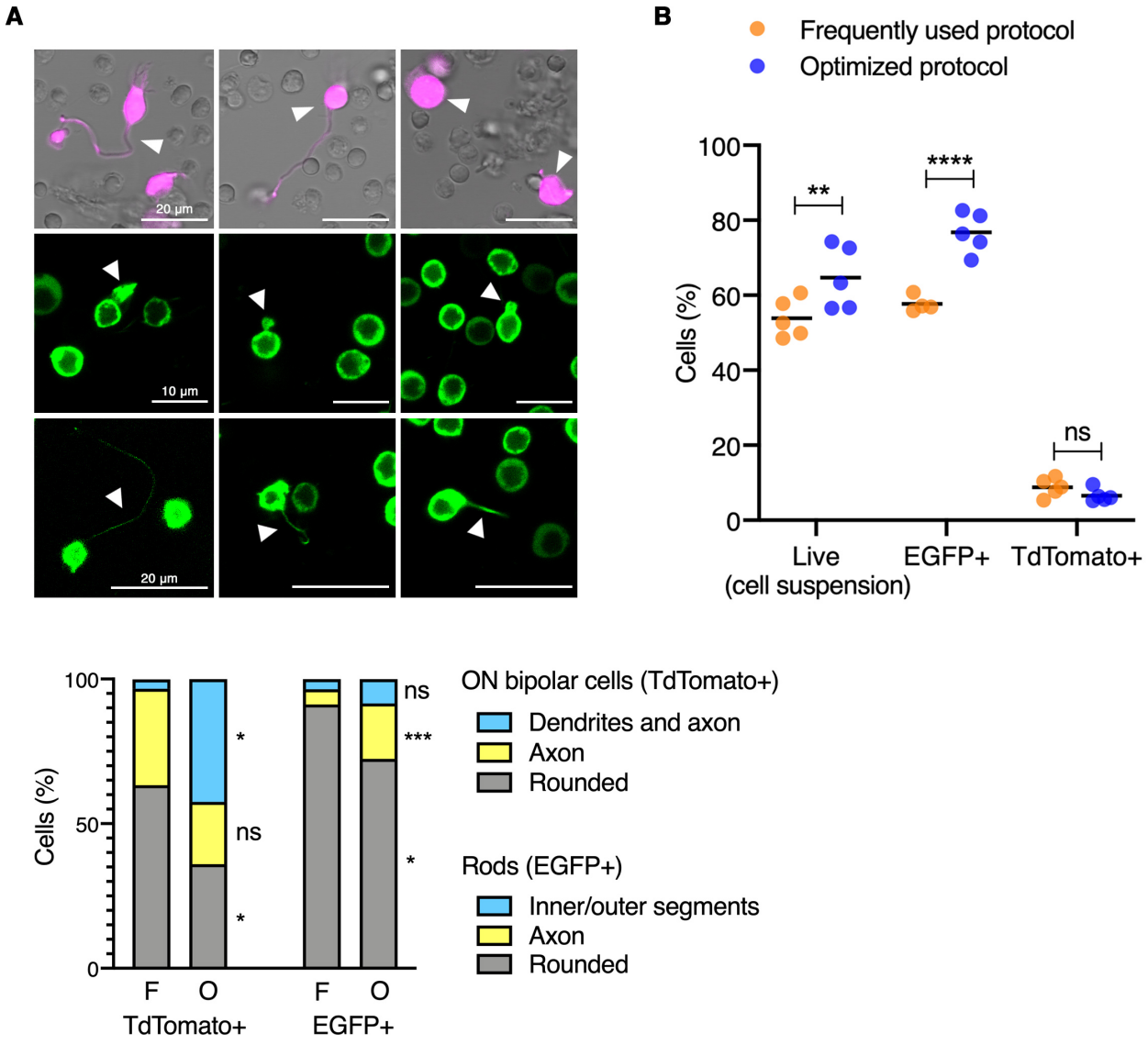

Figure 2. Morphometric and cytometric analyses of dissociated retinal cells. **A**: Morphometric analyses of rods and ON bipolar cells. The upper panel consists of nine confocal images representative of the distinct morphological categories that were followed for classifying rod and ON bipolar cells. First row: ON bipolar cells including dendrites, soma and axon (left), soma and axon (center), or with rounded shape (right). Second row: rods exhibiting inner or outer segments (length shrinkage observed). Third row: rod axons (short and thin). The stacked bar graph at the bottom shows the percentage of cells belonging to each morphological category for retinal cell suspensions obtained following the frequently used (F) or the optimized (O) protocol. A minimum of 200 cells per protocol and cell type were evaluated (2-3 biological replicates per protocol). Asterisks indicate significant differences between the two protocols for dissociation used: *p<0.05, ***p<0.001, two-way analysis of variance (ANOVA) multiple comparison test. ns: not significant. **B**: Flow cytometric analyses of retinal cell suspensions. Each dot represents the data of a biological replicate with n = 200,000 cells acquired, and black lines indicate the mean. Cell viability (live cells) was measured using 4′,6-diamidino-2-phenylindole (DAPI). Percentages of EGFP- and tdTomato-positive cells within each live cell population are shown. Asterisks indicate significant differences between the two protocols for dissociation used: **p<0.01, ****p<0.0001, two-way ANOVA multiple-comparison test. ns: not significant.

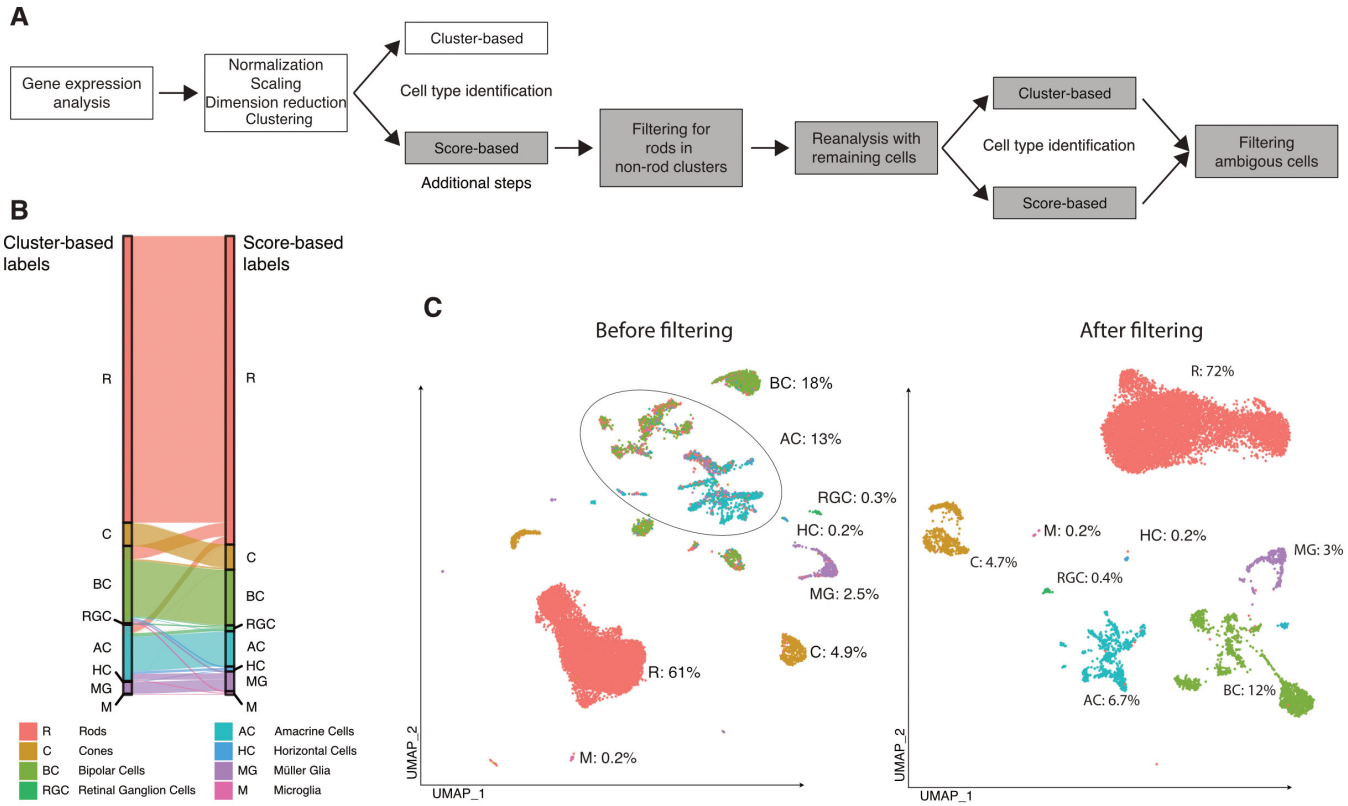

Figure 3. scRNA-seq analysis of retina samples. **A**: Flowchart showing the retina single-cell RNA sequencing (scRNA-seq) bioinformatic analysis pipeline. White boxes indicate commonly used steps. Gray boxes indicate additional steps included in the optimized protocol. **B**: Sankey plot of a published wild-type retina scRNA-seq data set (GEO accession # GSE125708). Left: cell type assignment by the frequently used cluster-based pipeline protocol. Right: cell type assignment by the optimized unsupervised score-based protocol. **C:** UMAP plots generated by scored-based cell type assignment information from (**B**), before and after additional filtering steps are applied. Cell clusters are colored based on the score-based cell-type assignment identical to (**B**). The circle in (**C**) marks clusters containing mixed cell types. Numbers indicate the proportion of the different cell types.

frequently used dissociation protocol. This same trend was observed in all retinal cell types (Figure 4C). Interestingly, only a small number of genes (33) were expressed in more than 50% of cells belonging to the same cell type in the cell suspensions prepared using the frequently used protocol for retina dissociation. Many of these genes are involved in stress-related responses (*Rnf187, Gsk3b, Lrp11*) and cell death (*Laptm4b, Mrfap1, Pdcd4*), or are indicators for low-quality cells, like mitochondrial or ribosomal genes. In addition, we compared the sensitivity of the latest 10x Genomics chemistry for 3′ gene expression analysis (v3.1, Figure 4D) with the version v2 (Figure 4B) using cell suspensions prepared following the optimized protocol for retina tissue dissociation. The v3.1 chemistry captured more genes per cell and increased the median of the genes detected per cell by about 500 in the different retinal cell populations compared to chemistry v2. Furthermore, the latest version of the chemistry (v3.1) allowed the capture of twice as many cells compared to chemistry v2 (4,500 cells/sample versus 1,500/sample; Figure 4G).

Most scRNA-seq studies examined freshly isolated cells. However, protocols compatible with fixation and freezing are emerging alternatives that facilitate the use of the scRNA-seq technique for clinical applications, developmental studies, or shipment of samples between collaborators. We evaluated the quality of the single-cell transcriptomes obtained from retinal cell suspensions fixed with methanol, as well as single nuclei suspensions prepared from frozen retinas (Figure 4E,F). The median number of genes detected per cell using methanol as a cell fixative was reduced by 500–1,000 genes compared to the median number of genes detected per cell using fresh tissue (Figure 4D,E). Among the different sample preparation protocols, nuclei suspensions yielded the lowest number of genes per cell captured, even with alignment of reads to a pre-mRNA reference (Figure 4F).

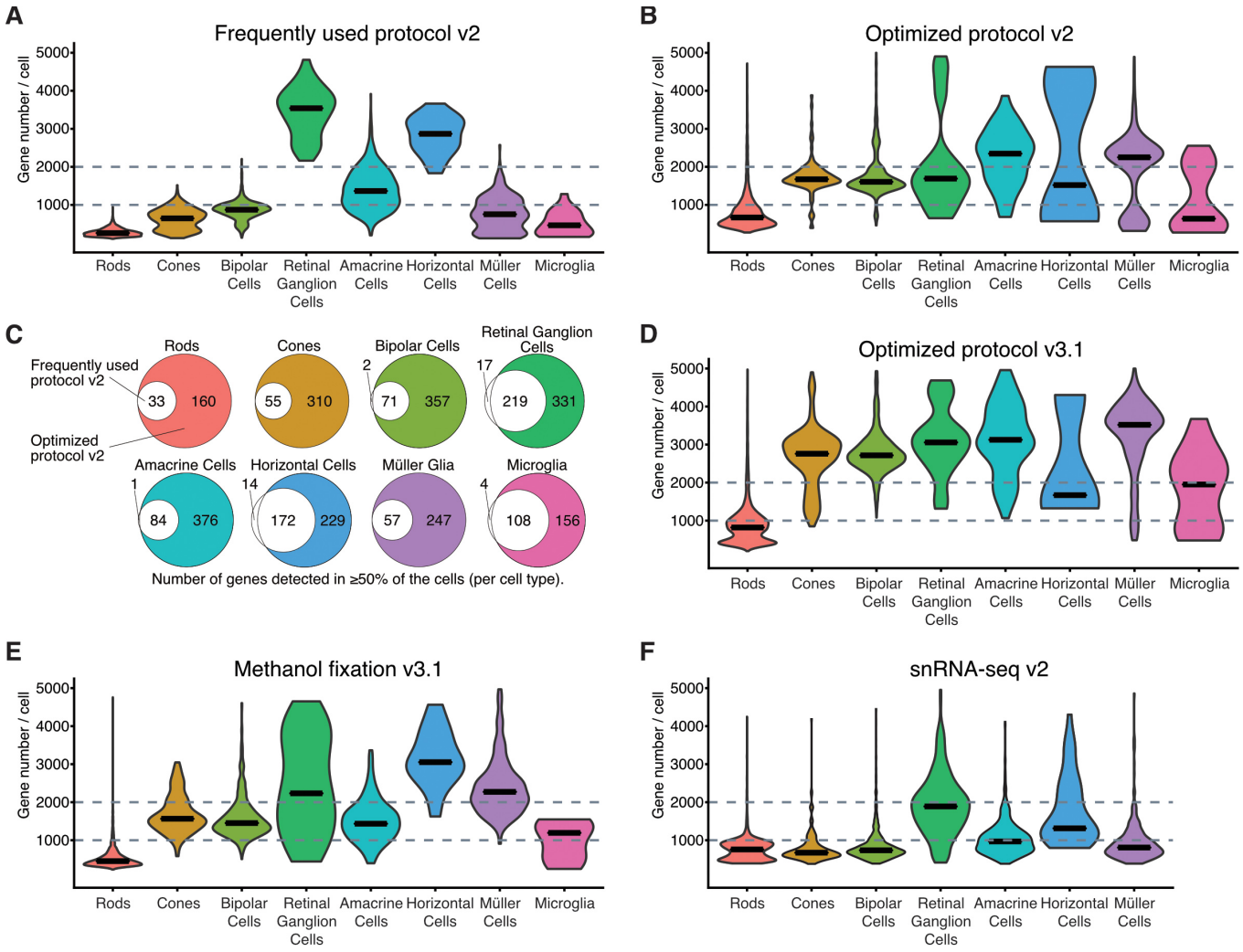

G

	# Total cells	% Rods	% Cones	% Bipolar Cells	% Retinal Ganglion Cells	% Amacrine Cells	% Horizontal Cells	% Müller Glia	% Micro-glia	# Replicates
Optimized protocol v2	4367	70.4	2.7	12.6	1.1	2	0.5	9.9	0.8	3
Optimized protocol v3.1	9025	77.7	3.2	10.9	0.3	1.3	0.2	6.1	0.3	2
Methanol fixation v3.1	7219	86.3	1.6	8.1	0.5	1.5	0.3	1.6	0.1	1
snRNA-seq v2	6437	51.6	4.8	17.8	3.9	15.8	0.7	5.5	0	1

Figure 4. Gene number per cell, detected with scRNA-seq using different sample preparation methods. **A**, **B**, **D**–**F**: Violin plots of genes detected per cell for each retinal cell type using fresh tissue dissociated with the frequently used protocol (**A**) and the optimized protocol (**B**, **D**), methanol fixed cells (**E**), and single nuclei suspensions (**F**). **C**: Euler diagrams showing the number of genes detected in the majority of the cells (≥50% of a particular cell type). White circles refer to data generated by the frequently used protocol (**A**). Colored circles refer to data generated using the optimized protocol (**B**). Colors are cell type matched. **G**: Table showing the total number of cells, proportion per cell type, and number of replicates. v2 corresponds to the use of Chromium Single Cell system chemistry Single Cell 3′ Library and Gel Bead Kit v2, whereas v3.1 indicates Single Cell 3′ GEM, Library and Gel Bead Kit v3.1.

Ambient RNA noise in retina samples: Finally, we assessed the amount of ambient rhodopsin mRNA, expressed in rod cells, contaminating non-rod cell populations across the different protocols. Rod cells are the predominant cell type in the mouse retina, accounting for more than 70% of all cells. Damage to rod cell cilium during dissociation resulting in the release of ambient rhodopsin mRNA into the cell suspension is the major cause of cross-contamination in retina samples. Between the two 10x Genomics chemistry versions, the level of rhodopsin contamination was lower using the latest chemistry available (v3.1) compared to the previous one (v2; Figure 5A). The results exhibited a slight decrease in rhodopsin contamination in the fixed cell samples compared to the unfixed cells, likely attributed to the additional washing steps in the protocol (Figure 5A,B). The highest rod contamination among all the samples was observed in the snRNA-seq sample, where rhodopsin expression was surprisingly high and homogeneous in non-rod cell populations (Figure 5C).

DISCUSSION

Distinct cell types and their subtypes in the mammalian retina have been defined based on morphology, function, or the expression of a limited number of genes [33]. Recent advances in single-cell RNA sequencing technologies have enabled the characterization of transcriptome profiles of individual cells making it possible to map developmental trajectories, subtype diversity, and putative causal genes of retinal pathologies [6,7,9,13,14,16,34]. However, the scRNA-seq technique includes challenges of tissue dissociation into a single cell suspension and biases of transcript coverage for highly expressed genes, which constitute important limitations for mouse retinal studies due to the abundance of rod photoreceptors and their opsin expression-dominated transcriptome. In this report, we described an optimized dissociation protocol and bioinformatic pipeline for the analysis of scRNA-seq of retinal samples.

We introduced a gentle protocol for retina dissociation that reduces the enzymatic activity of papain by incubating the retinal tissue at lower temperatures compared to frequently used protocols. In addition, we used flame polished glass Pasteur pipettes for tissue trituration, which decreased the resistance of the solution flow and put less stress on the sample. We also added a cocktail of antioxidants to the solutions used for tissue dissociation. Consequently, we showed that this protocol defines a better single-cell transcriptional landscape compared to published protocols for retina samples, being able to detect a higher number of genes per cell (up to a fourfold increase). The protocol introduced fewer artifactual gene expression changes compared to those induced by proteolytic digestion at higher temperatures. We

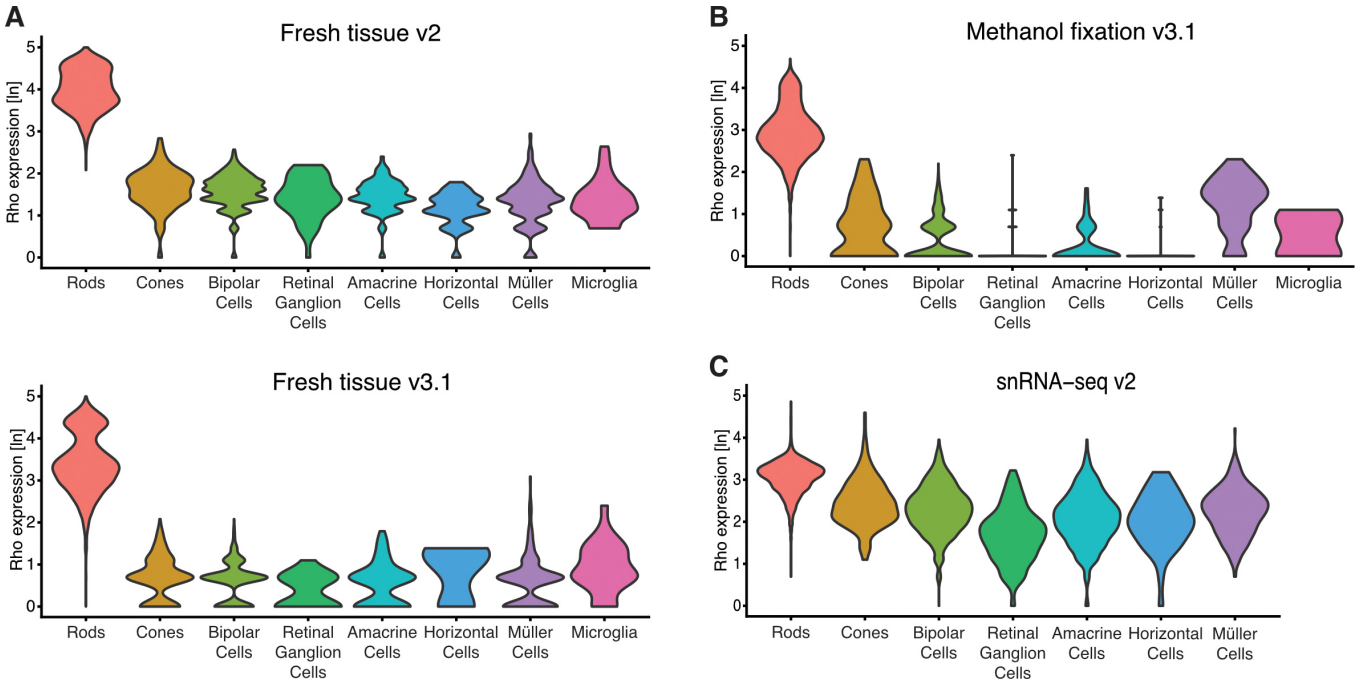

Figure 5. Ambient RNA noise in scRNA-seq retina samples. **A**–**C**: Violin plots showing the natural logarithm of rhodopsin (*Rho*) expression per cell type in fresh tissue (**A**), methanol fixed cells (**B**), and single nuclei suspensions (**C**). v2 corresponds to the use of Chromium Single Cell system chemistry Single Cell 3′ Library and Gel Bead Kit v2, whereas v3.1 indicates Single Cell 3′ GEM, Library and Gel Bead Kit v3.1.

detected expression of immediate-early genes and those associated with stress responses and cell death processes that were unique to the sample prepared following the commonly used protocol. These findings are concordant with previous studies that demonstrated induction of stress response–related genes in tissues dissociated at 37 °C [35-37]. In this regard, it could be interesting to explore the use of psychrophilic proteases in retinal dissociation protocols. This would allow the entire tissue dissociation process to be performed in ice, in which mammalian transcriptional machinery shows little activity, thus minimizing gene expression artifacts. However, the optimized protocol might not fully encompass the transcriptome landscape of cells in the inner retina (e.g., horizontal, amacrine, microglia, and retinal ganglion cells) due to the high abundance of rods in the mouse retina and the low capture efficiency of the scRNA-seq technique. Thus, depletion of rods may be necessary to study inner retinal cells or to enrich samples in specific cell types after the tissue dissociation protocol, as demonstrated recently [8]. In addition to the mouse retina, we applied the optimized dissociation protocol successfully to human retina samples and retinal organoids, with minor modifications of the incubation time with the enzyme. The data also revealed a decrease in ambient RNA contamination levels using the most recent 10x Genomics chemistry version (v3.1) compared to v2 in cell suspensions prepared following the same protocol. This could be attributed to microcapillary design differences between the Chromium single-cell chips used in the different chemistry versions. The encapsulation of cells in water-in-oil droplets in the chip used for the v3.1 chemistry likely causes less cell damage compared to the chip used for chemistry v2.

To reduce the noise caused by ambient RNA and low-quality cells from the retina samples, we optimized the in silico bioinformatic pipeline by adding extra filtering steps to the automatic cell identification methods. However, ambient RNA is not the only source of false positive gene detection. Multiplets are generated when two or more cells are incorporated together in the same microfluidic droplet. Heterotypic multiplets have an unusually high gene number but also show mixed cell type gene expression. We refrained from filtering for typical quality control hallmarks, like gene number per cell or percentage of mitochondrial reads, because the retina is one of the most metabolically active tissues [38] and naturally differs in RNA content and number of mitochondria. We believe that the proposed score-based pipeline to identify cell types might not be appropriate for diseased or degenerating retinas in which the expression profiles for cells may be altered but physiologically significant.

The full potential of scRNA-seq can be realized with fresh tissue samples. However, additional restrictions and challenges are faced by experimental designs where samples cannot be processed immediately. In this case, fixation of cell suspensions with methanol or tissue sample snap-freezing offer alternative solutions. We observed an overall reduction in gene number detected per cell for most of cell types in the scRNA-seq data from the methanol fixed cells and in snRNA-seq data from isolated nuclei, obtained from frozen tissues. Based on these results, and considering the amount of ambient RNA contamination in the snRNA-seq data, we recommend choosing methanol fixed cell suspensions over single nuclei cell suspensions when fresh dissociated tissue is not an experimental option.

In summary, the results emphasize the relevance of good quality cell or nuclei suspensions to generate accurate and reliable gene expression data sets. It is important to optimize the dissociation protocol and single-cell method before undertaking large-scale experiments, as well as to adapt bioinformatic pipelines to different tissues. The protocol described in this work may be useful for comparative analysis in other ocular tissues with single gene or cell type dominance [39].

DATA AVAILABILITY: The data reported here are available in the Gene Expression Omnibus (GEO) database (accession # GSE153674).

ACKNOWLEDGMENTS

We sincerely thank Scott Henke, Megan Kopera, Jessica D. Gumerson and Arturo Rivera for assistance with mouse lines and genotyping, Zachary Batz for GEO submission of sequencing data, and Nicolás Cuenca, Francisco M. Nadal-Nicolás and Maria de los Angeles Jaime for helpful discussions. We are grateful to Dr. Rachel O. Wong (University of Washington, Seattle) for providing us with *mGluR6-tdTomato* mice. This research was supported by the Intramural Research Programs of the National Eye Institute (ZIAEY000450 and ZIAEY000546 to A.S.) and the National Institute on Deafness and Other Communication Disorders (ZIC DC000086 to the Genomics and Computational Biology Core), National Institutes of Health. This work used the high-performance computational capabilities of the NIH Biowulf Linux cluster (NIH). CCR Single Cell Analysis Facility was supported by FNLCR Contract HHSN261200800001E. Dr. Anand Swaroop (swaroopa@nei.nih.gov) and Dr. Laura Campello (laura.campello@nih.gov) should be considered co-corresponding authors for this study.

REFERENCES

1. Mortazavi A, Williams BA, McCue K, Schaeffer L, Wold B. Mapping and quantifying mammalian transcriptomes by RNA-Seq. Nat Methods 2008; 5:621-8. [PMID: 18516045].
2. Wang Z, Gerstein M, Snyder M. RNA-Seq: a revolutionary tool for transcriptomics. Nat Rev Genet 2009; 10:57-63. [PMID: 19015660].
3. Marioni JC, Mason CE, Mane SM, Stephens M, Gilad Y. RNA-seq: an assessment of technical reproducibility and comparison with gene expression arrays. Genome Res 2008; 18:1509-17. [PMID: 18550803].
4. Ramskold D, Luo S, Wang YC, Li R, Deng Q, Faridani OR, Daniels GA, Khrebtukova I, Loring JF, Laurent LC, Schroth GP, Sandberg R. Full-length mRNA-Seq from single-cell levels of RNA and individual circulating tumor cells. Nat Biotechnol 2012; 30:777-82. [PMID: 22820318].
5. Macosko EZ, Basu A, Satija R, Nemesh J, Shekhar K, Goldman M, Tirosh I, Bialas AR, Kamitaki N, Martersteck EM, Trombetta JJ, Weitz DA, Sanes JR, Shalek AK, Regev A, McCarroll SA. Highly Parallel Genome-wide Expression Profiling of Individual Cells Using Nanoliter Droplets. Cell 2015; 161:1202-14. [PMID: 26000488].
6. Lukowski SW, Lo CY, Sharov AA, Nguyen Q, Fang L, Hung SS, Zhu L, Zhang T, Grunert U, Nguyen T, Senabouth A, Jabbari JS, Welby E, Sowden JC, Waugh HS, Mackey A, Pollock G, Lamb TD, Wang PY, Hewitt AW, Gillies MC, Powell JE, Wong RC. A single-cell transcriptome atlas of the adult human retina. EMBO J 2019; 38:e100811-[PMID: 31436334].
7. Sridhar A, Hoshino A, Finkbeiner CR, Chitsazan A, Dai L, Haugan AK, Eschenbacher KM, Jackson DL, Trapnell C, Bermingham-McDonogh O, Glass I, Reh TA. Single-Cell Transcriptomic Comparison of Human Fetal Retina, hPSC-Derived Retinal Organoids, and Long-Term Retinal Cultures. Cell Reports 2020; 30:1644-59. [PMID: 32023475].
8. Peng YR, Shekhar K, Yan W, Herrmann D, Sappington A, Bryman GS, van Zyl T, Do MTH, Regev A, Sanes JR. Molecular Classification and Comparative Taxonomics of Foveal and Peripheral Cells in Primate Retina. Cell 2019; 176:1222-37. [PMID: 30712875].
9. Menon M, Mohammadi S, Davila-Velderrain J, Goods BA, Cadwell TD, Xing Y, Stemmer-Rachamimov A, Shalek AK, Love JC, Kellis M, Hafler BP. Single-cell transcriptomic atlas of the human retina identifies cell types associated with age-related macular degeneration. Nat Commun 2019; 10:4902-[PMID: 31653841].
10. Collin J, Queen R, Zerti D, Dorgau B, Hussain R, Coxhead J, Cockell S, Lako M. Deconstructing Retinal Organoids: Single Cell RNA-Seq Reveals the Cellular Components of Human Pluripotent Stem Cell-Derived Retina. Stem Cells 2019; 37:593-8. [PMID: 30548510].
11. Kim S, Lowe A, Dharmat R, Lee S, Owen LA, Wang J, Shakoor A, Li Y, Morgan DJ, Hejazi AA, Cvekl A, DeAngelis MM, Zhou ZJ, Chen R, Liu W. Generation, transcriptome profiling, and functional validation of cone-rich human retinal organoids. Proc Natl Acad Sci USA 2019; 116:10824-33. [PMID: 31072937].
12. Mao X, An Q, Xi H, Yang XJ, Zhang X, Yuan S, Wang J, Hu Y, Liu Q, Fan G. Single-Cell RNA Sequencing of hESC-Derived 3D Retinal Organoids Reveals Novel Genes Regulating RPC Commitment in Early Human Retinogenesis. Stem Cell Reports 2019; 13:747-60. [PMID: 31543471].
13. Clark BS, Stein-O'Brien GL, Shiau F, Cannon GH, Davis-Marcisak E, Sherman T, Santiago CP, Hoang TV, Rajaii F, James-Esposito RE, Gronostajski RM, Fertig EJ, Goff LA, Blackshaw S. Single-Cell RNA-Seq Analysis of Retinal Development Identifies NFI Factors as Regulating Mitotic Exit and Late-Born Cell Specification. Neuron 2019; 102:1111-26. [PMID: 31128945].
14. Shekhar K, Lapan SW, Whitney IE, Tran NM, Macosko EZ, Kowalczyk M, Adiconis X, Levin JZ, Nemesh J, Goldman M, McCarroll SA, Cepko CL, Regev A, Sanes JR. Comprehensive Classification of Retinal Bipolar Neurons by Single-Cell Transcriptomics. Cell 2016; 166:1308-23. [PMID: 27565351].
15. Daniszewski M, Senabouth A, Nguyen QH, Crombie DE, Lukowski SW, Kulkarni T, Sluch VM, Jabbari JS, Chamling X, Zack DJ, Pebay A, Powell JE, Hewitt AW. Single cell RNA sequencing of stem cell-derived retinal ganglion cells. Sci Data 2018; 5:180013-[PMID: 29437159].
16. Rheaume BA, Jereen A, Bolisetty M, Sajid MS, Yang Y, Renna K, Sun L, Robson P, Trakhtenberg EF. Single cell transcriptome profiling of retinal ganglion cells identifies cellular subtypes. Nat Commun 2018; 9:2759-[PMID: 30018341].
17. Heng JS, Rattner A, Stein-O'Brien GL, Winer BL, Jones BW, Vernon HJ, Goff LA, Nathans J. Hypoxia tolerance in the Norrin-deficient retina and the chronically hypoxic brain studied at single-cell resolution. Proc Natl Acad Sci USA 2019; 116:9103-14. [PMID: 30988181].
18. Ronning KE, Karlen SJ, Miller EB, Burns ME. Molecular profiling of resident and infiltrating mononuclear phagocytes during rapid adult retinal degeneration using single-cell RNA sequencing. Sci Rep 2019; 9:4858-[PMID: 30890724].
19. Phillips MJ, Jiang P, Howden S, Barney P, Min J, York NW, Chu LF, Capowski EE, Cash A, Jain S, Barlow K, Tabassum T, Stewart R, Pattnaik BR, Thomson JA, Gamm DM. A Novel Approach to Single Cell RNA-Sequence Analysis Facilitates In Silico Gene Reporting of Human Pluripotent Stem Cell-Derived Retinal Cell Types. Stem Cells 2018; 36:313-24. [PMID: 29230913].
20. Yan W, Peng YR, van Zyl T, Regev A, Shekhar K, Juric D, Sanes JR. Cell Atlas of The Human Fovea and Peripheral Retina. Sci Rep 2020; 10:9802-[PMID: 32555229].
21. Kolb H. Simple Anatomy of the Retina. In: Kolb H, Fernandez E, Nelson R, editors. Webvision: The Organization of the Retina and Visual System. Salt Lake City (UT)1995.
22. Dowling JE. The retina. An Approchable Part of the Brain. Cambridge, Harvard University Press 1987.

23. Kennedy B, Malicki J. What drives cell morphogenesis: a look inside the vertebrate photoreceptor. Dev Dyn 2009; 238:2115-38. [PMID: 19582864].

24. Akimoto M, Cheng H, Zhu D, Brzezinski JA, Khanna R, Filippova E, Oh EC, Jing Y, Linares JL, Brooks M, Zareparsi S, Mears AJ, Hero A, Glaser T, Swaroop A. Targeting of GFP to newborn rods by Nrl promoter and temporal expression profiling of flow-sorted photoreceptors. Proc Natl Acad Sci USA 2006; 103:3890-5. [PMID: 16505381].

25. Kerschensteiner D, Morgan JL, Parker ED, Lewis RM, Wong RO. Neurotransmission selectively regulates synapse formation in parallel circuits in vivo. Nature 2009; 460:1016-20. [PMID: 19693082].

26. Chen J, Cheung F, Shi R, Zhou H, Lu W, Consortium CHI. PBMC fixation and processing for Chromium single-cell RNA sequencing. J Transl Med 2018; 16:198-[PMID: 30016977].

27. Matson KJE, Sathyamurthy A, Johnson KR, Kelly MC, Kelley MW, Levine AJ. Isolation of Adult Spinal Cord Nuclei for Massively Parallel Single-nucleus RNA Sequencing. J Vis Exp 2018; •••:140-[PMID: 30371670].

28. Butler A, Hoffman P, Smibert P, Papalexi E, Satija R. Integrating single-cell transcriptomic data across different conditions, technologies, and species. Nat Biotechnol 2018; 36:411-20. [PMID: 29608179].

29. Stuart T, Butler A, Hoffman P, Hafemeister C, Papalexi E, Mauck WM 3rd, Hao Y, Stoeckius M, Smibert P, Satija R. Comprehensive Integration of Single-Cell Data. Cell 2019; 177:1888-902. [PMID: 31178118].

30. Hafemeister C, Satija R. Normalization and variance stabilization of single-cell RNA-seq data using regularized negative binomial regression. Genome Biol 2019; 20:296-[PMID: 31870423].

31. Wang J, O'Sullivan ML, Mukherjee D, Punal VM, Farsiu S, Kay JN. Anatomy and spatial organization of Muller glia in mouse retina. J Comp Neurol 2017; 525:1759-77. [PMID: 27997986].

32. Jeon CJ, Strettoi E, Masland RH. The major cell populations of the mouse retina. J Neurosci 1998; 18:8936-46. [PMID: 9786999].

33. Masland RH. The neuronal organization of the retina. Neuron 2012; 76:266-80. [PMID: 23083731].

34. Orozco LD, Chen HH, Cox C, Katschke KJ Jr, Arceo R, Espiritu C, Caplazi P, Nghiem SS, Chen YJ, Modrusan Z, Dressen A, Goldstein LD, Clarke C, Bhangale T, Yaspan B, Jeanne M, Townsend MJ, van Lookeren Campagne M, Hackney JA. Integration of eQTL and a Single-Cell Atlas in the Human Eye Identifies Causal Genes for Age-Related Macular Degeneration. Cell Reports 2020; 30:1246-59. [PMID: 31995762].

35. Adam M, Potter AS, Potter SS. Psychrophilic proteases dramatically reduce single-cell RNA-seq artifacts: a molecular atlas of kidney development. Development 2017; 144:3625-32. [PMID: 28851704].

36. van den Brink SC, Sage F, Vertesy A, Spanjaard B, Peterson-Maduro J, Baron CS, Robin C, van Oudenaarden A. Single-cell sequencing reveals dissociation-induced gene expression in tissue subpopulations. Nat Methods 2017; 14:935-6. [PMID: 28960196].

37. Denisenko E, Guo BB, Jones M, Hou R, de Kock L, Lassmann T, Poppe D, Clement O, Simmons RK, Lister R, Forrest ARR. Systematic assessment of tissue dissociation and storage biases in single-cell and single-nucleus RNA-seq workflows. Genome Biol 2020; 21:130-[PMID: 32487174].

38. Wong-Riley M. Energy metabolism of the visual system. Eye Brain 2010; 2:99-[PMID: 23226947].

39. Wagner AH, Anand VN, Wang WH, Chatterton JE, Sun D, Shepard AR, Jacobson N, Pang IH, Deluca AP, Casavant TL, Scheetz TE, Mullins RF, Braun TA, Clark AF. Exon-level expression profiling of ocular tissues. Exp Eye Res 2013; 111:105-11. [PMID: 23500522].

Articles are provided courtesy of Emory University and the Zhongshan Ophthalmic Center, Sun Yat-sen University, P.R. China. The print version of this article was created on 10 October 2020. This reflects all typographical corrections and errata to the article through that date. Details of any changes may be found in the online version of the article.